JOURNAL OF GUIDANCE, CONTROL, AND DYNAMICS
Vol. 18, No. 4, July–August 1995

Closed Loop Momentum Transfer Maneuvers Using Multiwheels

Jun'ichiro Kawaguchi*
Institute of Space and Astronautical Science, Sagamihara, Kanagawa 229, Japan
Ken Maeda†
NEC Aerospace Systems, Ltd., Kouhoku, Yokohama 222, Japan
and
Hiroki Matsuo‡ and Keiken Ninomiya§
Institute of Space and Astronautical Science, Sagamihara, Kanagawa 229, Japan

This paper proposes a control law that stabilizes a momentum transfer maneuver using multiwheels, which provides an analytical proof via Lyapunov's direct method. Since an open-loop transfer sometimes causes divergent and large nutation motion, especially when a minor to major axis transfer is attempted, the closed-loop scheme is discussed here. This paper also points out equilibrium "singular states" which may occur not only in open loop but also in a closed-loop momentum transfer, from which no evasive path can be found. This paper provides sufficient conditions by which both divergent behavior and singular states can be circumvented by appropriately selecting the control law proposed here or by use of inertia properties of the spacecraft. This may be the most distinct feature of a closed-loop transfer utilizing multiwheels vs conventional open-loop schemes. This paper shows that neither the open-loop method nor closed-loop control with a single wheel system avoids these undesirable phenomena. The proposed control scheme with four wheels is numerically demonstrated to improve significantly the transfer behavior and exclude any singular state occurrence.

Nomenclature

C = $3 \times n$ matrix whose jth column indicates orientation of 2_j axis in S_b frame
C_{bj} = coordinate transformation matrix from S_{wj} to S_b
$\boldsymbol{C}_{2j}$ = unit vector along 2_j axis
$\boldsymbol{H}_b$ = angular momentum vector of spacecraft core body with respect to the center of mass of entire system
$\boldsymbol{H}_T$ = total angular momentum vector of spacecraft with n wheels
$\boldsymbol{H}_w$ = total angular momentum vector of all wheels around their 2_j axes
$\boldsymbol{H}_{wf}$ = angular momentum vector commanded
H_0 = total angular momentum of spacecraft, $=|\boldsymbol{H}_T|$
$\boldsymbol{h}_j$ = angular momentum vector of the jth wheel in wheel fixed frame, $j = 1, \ldots, n$
I_w = rotational moment of inertia of each wheel around its 2_j axis
J = inertia tensor of spacecraft with n wheels
J_b = inertia tensor of spacecraft core body excluding wheels
J_{ij} = $i_b - j_b$ cross product component of J_s
J_{ik} = elements of matrix J_s, $i, k = 1, 2, 3$
J_r = diagonal matrix composed of J_{rj}: diag$(J_{r1}, \ldots, J_{rn})$
J_{rj} = moment of inertia about rotor (2_j) axis of the jth wheel
J_s = inertia tensor of body and the wheels excluding the inertia about the rotor (2_j) axes
J_{tj} = moment of inertia about transversal axis $(1_j, 3_j$ axes) of the jth wheel
J_{wj} = inertia tensor of the jth wheel, $j = 1, \ldots, n$
J'_{wj} = inertia tensor of the jth wheel excluding rotor axis component, $j = 1, \ldots, n$
K = scalar gain that appears in the control scheme defined in Eq. (13)
K_a = scalar control parameter for body rate
K_b = scalar control parameter for wheel rate with respect to inertial frame
M_j = mass of the jth wheel
R_j = bearing suspension torque of the jth wheel excluding friction torque
$\boldsymbol{r}_j$ = position vector of the center of mass of the jth wheel from center of mass of entire system
S_b = coordinate system fixed in the body of the spacecraft, whose origin coincides with the center of mass of entire spacecraft system
S_{wj} = coordinate system fixed in the jth wheel
$\boldsymbol{T}$ = torque vector driving n wheels
$\boldsymbol{T}_j$ = torque vector applied to the 2_j axis
T_j = elements of $\boldsymbol{T}$, $j = 1, \ldots, n$
α = complement elevation angle of rotor axes
β = angles that define rotor axes together with α angles
γ = elevation angle of wheel rotor axis measured from the plane defined by 1_b and 3_b axes
Ω = set of spin rate vectors of all wheels with respect to S_b
Ω_f = ultimate spin rate command for the wheels
$\boldsymbol{\Omega}_j$ = spin rate vector of the jth wheel with respect to S_b
Ω_j = elements of $\boldsymbol{\Omega}$, $j = 1, \ldots, n$
$\boldsymbol{\omega}$ = angular rate vector of S_b with respect to inertial frame
$\mathbf{1}$ = unit matrix
$1_b, 2_b, 3_b$ = direction of axes that span body-fixed coordinate in parallel with the principal axes of spacecraft core body, X, Y, Z axes in S_b
$1_j, 2_j, 3_j$ = direction of axes that span the jth wheel-fixed coordinate in parallel with the principal axes of wheel j, X, Y, Z axes in S_{wj}
$(*)$ = singular state

Presented as Paper 92-4332 at the AIAA Guidance, Navigation, and Control Conference, Hilton Head, SC, Aug. 10–12, 1992; received Jan. 19, 1993; revision received May 17, 1994; accepted for publication Dec. 15, 1994.

*Associate Professor, Systems Engineering, 3-1-1 Yoshinodai. Member AIAA.
†Engineering Manager, 2-4-18 Shinyokohama.
‡Professor, Systems Engineering, 3-1-1 Yoshinodai.
§Professor, Spacecraft Control, 3-1-1 Yoshinodai.

Introduction

MOMENTUM transfer schemes which have been frequently utilized convert the angular momentum vector around one axis to that around another axis, such as the principal axis with maximum moment of inertia. The original axis may be the initial spin

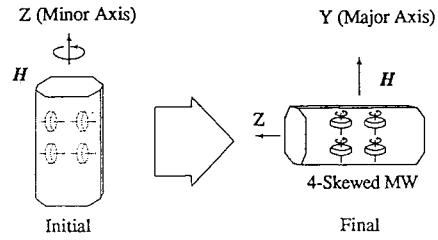

Fig. 1 Fundamental concept of momentum transfer.

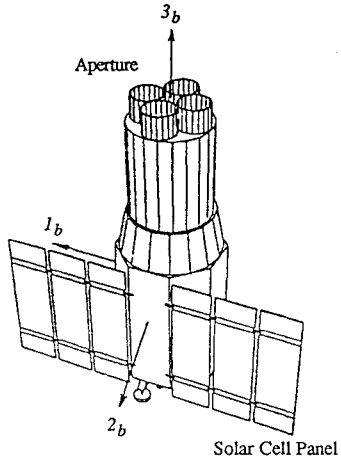

Fig. 2 Schematic drawing of ASTRO-D spacecraft.

axis, which is often constrained by the launch vehicle configuration. The fundamental concept of a momentum transfer scheme is shown in Fig. 1. There is a straightforward solution to the problem of momentum transfer from the minimum moment of inertia case to the maximum moment of inertia case, such as an orthogonal transfer where the initial angular momentum vector direction is identical to the spin or the Z axis to the final angular momentum vector along the Y axis. This conversion is accomplished by spinning up the internal wheels to an appropriate level. There are many studies concerning the stability of such maneuvers when only a single-wheel configuration without closed-loop control is used, although few discussions have focused their attention on the case of closed control with multiwheels. This paper will show that closed control with a single wheel is not as beneficial as using multiwheels, since it does not compensate for unfavorable inertia properties.

The Institute of Space and Astronautical Science (ISAS) is in charge of launching and operating scientific spacecraft in Japan and launch of the ASTRO-D x-ray telescope spacecraft was scheduled for February, 1993. ASTRO-D required extremely high-attitude stability and, therefore, carries four wheels. A schematic drawing of the ASTRO-D spacecraft is depicted in Fig. 2. In this spacecraft, the solar cell panels would be pointed toward the sun, and the angular momentum vector would be aligned with Y axis. Since ASTRO-D's launch vehicle configuration required the initial spin axis be prescribed as the Z axis with minimum moment of inertia, a momentum transfer scheme was planned. Since 1982, at least five spacecraft performed minimum-to-maximum momentum transfers with the conventional open-loop transfer scheme, although it does not seem to fit this maneuver type very well. As stated, ASTRO-D requires a transfer from minimum to maximum momentum. Numerical analysis suggested that an open-loop scheme does not accomplish the transfer fast and efficiently, therefore, a closed-loop control was introduced so as to secure the maneuver. Figure 3 illustrates initial acquisition sequences assumed for the ASTRO-D satellite. The initial spin direction is frozen and defined by the launch vehicle's upper stage, so that a momentum transfer maneuver enables sun acquisition control as well as solar cell deployment.

This paper proposes a new closed-loop control law that stabilizes the minimum-to-maximum momentum transfer maneuver using four wheels, whose stability is proved analytically via Lyapunov's direct method. Historically speaking, the attitude motion for a class

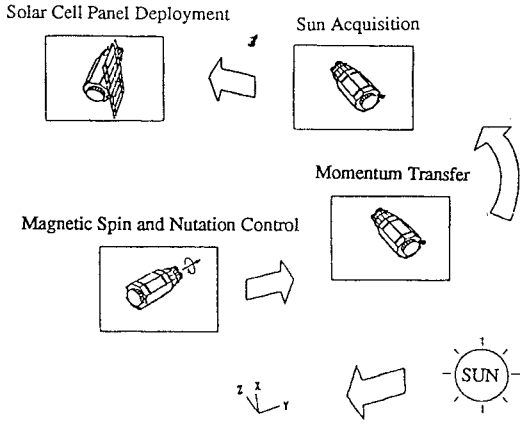

Fig. 3 Initial attitude acquisition sequences.

of dual-spin spacecraft has been of particular concern, and the nonlinear, internal resonances during the despin process was intensively investigated.[1,2] Resonance conditions as well as the near-resonant motion were clarified[2] with an exact analytical solution for an asymmetric gyrostat.[3] In 1974, Scher and Farrenktopf[4] reported that two equilibrium trap states exist in dual-spin spacecraft dynamics. Excitation by the motor was found to lead to escape from those traps. A similar case of flat spin recovery behavior with a rotor was studied[5] and it was found that the residual nutation angle is affected by the spacecraft inertia properties. In 1981, Hubert[6] proposed the generalized dual-spin turn technique followed by passive energy dissipation, which orients the rotor axis of a dual-spin spacecraft parallel to the total angular momentum vector. A discussion on the number of equilibrium points and their locations has been generalized and presented in Refs. 6 and 7. As for the closed control scheme, in 1989 Guelman[8] developed a two-step control strategy. Its control sequence assumes the trajectory first falling into the special equilibrium state, from which a constant torque is then applied so that the spacecraft attitude is recovered. From the beginning of the ASTRO-D program, the feasibility of this momentum transfer technique has been examined,[9,10] and a closed control scheme that accomplishes the maneuver has been devised.[11–13]

Past discussions on momentum transfer via a single wheel generally concluded that six equilibrium states exist during spin up of a wheel, which is in agreement with the results obtained here. Whether those singular states exist or not is dependent only on the spacecraft inertia property in the open-loop transfer, and it was revealed that only a major to minor axis transfer is practical without any passive damping, therefore, is preferable. At the beginning phase of transfer, in addition to singularities, unexpected divergent motion sometimes takes place, which was also accounted for by Hubert.[6] Consequently, there are two kinds of possible failures modes in a conventional transfer: divergent nutation motion and singular equilibrium states, both of which are not avoided by the open-loop methods but are governed only by spacecraft inertia property. Except for Ref. 8, little effort has been expended in overcoming these difficulties, and this paper may be the first that discusses the advantages of using closed-loop control utilizing multiwheels. This paper will discuss these phenomena from this new aspect, expanding the maneuver incorporating the closed-loop control. What is new here is, first of all, that equilibrium states are expressed explicitly in terms of control parameters as well as inertia properties. Second, sufficient conditions are analytically given, in which either appropriate choice of control law or inertia properties circumvents both singular states and divergent motion associated with the transfer. It is noted that closed control in a single wheel system is not of much practical use, since it does not improve the inertia property. What is of consequence is the requirement on the wheel configuration; not all multiwheel configurations are effective to this end.

Numerical examples are shown for the ASTRO-D spacecraft, which demonstrate closed-control features in a momentum transfer. First of all, it will be shown that the transfer fails and falls into an equilibrium singular state when it is performed via a conventional open-loop scheme. A simulation using energy dissipation suggests

that the equilibrium point is not a final destination and that transfer is accomplished over quite a long period. Subsequent simulations exhibiting appropriate choice of control parameters avoids both singular states and divergent motion and completes acquisition quickly compared to the energy dissipation case. All of these results prove the proposed control law will work satisfactorily in the ASTRO-D mission. The actual flight results are also shown, in which perfect compensation was given up having taken the hardware circuits and sensor noises into account. However, the maneuver was carried out successfully in accordance with the analyses developed here and the proposed strategy here was well supported by the flight.

Equations of Motion in the Spacecraft with Multiwheels

The spacecraft with multiwheels to be analyzed consists of a rigid body and n wheels with symmetric rotors. The $n+1$ orthogonal coordinate systems S_b and S_{wj} $(j = 1, 2, \ldots, n)$ are defined. The rotor axis of the jth wheel is defined along the 2_j axis in S_{wj} without loss of generality as shown in Fig. 4. Note that all of the wheels are assumed symmetric around their spin axes and that the center of mass of the entire system never shifts even while the wheels are spinning. Here it is also assumed that the wheel axes are configured so that the principal axes of the entire spacecraft coincide with those of spacecraft core body itself. Core body angular momentum is written in S_b as

$$\boldsymbol{H}_b = J_b\boldsymbol{\omega} \tag{1}$$

A momentum of the jth wheel measured in S_{wj} relative to the inertial space can be expressed as

$$J_{wj}C_{jb}\boldsymbol{\omega} + \boldsymbol{h}_j, \qquad J_{wj} = J'_{wj} + J_{rj}\begin{bmatrix}000\\010\\000\end{bmatrix} \tag{2}$$

where $\boldsymbol{h}_j$ has a nonzero component only in the 2_j direction as follows:

$$\boldsymbol{h}_j = J_{wj}\boldsymbol{\Omega}_j = \begin{bmatrix}0\\J_{rj}\Omega_j\\0\end{bmatrix} \tag{3}$$

The total angular momentum of the spacecraft with n wheels is written as

$$\begin{aligned}&\boldsymbol{H}_T = J_s\boldsymbol{\omega} + \boldsymbol{H}_w, \qquad \boldsymbol{H}_w = CJ_rC^T\boldsymbol{\omega} + CJ_r\boldsymbol{\Omega}\\ &J_s = J_b + \sum_j^n C_{bj}J'_{wj}C_{jb} + \sum_j^n M_j\left(\boldsymbol{r}_j^T\boldsymbol{r}_j\mathbf{1} - \boldsymbol{r}_j\boldsymbol{r}_j^T\right)\end{aligned} \tag{4}$$

Assuming no external torque on the spacecraft, the dynamic equations of the entire spacecraft with n wheels can be written as follows:

$$\begin{aligned}&\dot{\boldsymbol{H}}_T + \boldsymbol{\omega}\times\boldsymbol{H}_T = 0\\ &J_{wj}(C_{jb}\dot{\boldsymbol{\omega}} + \dot{\boldsymbol{\Omega}}_j) + (C_{jb}\boldsymbol{\omega} + \boldsymbol{\Omega}_j)\times J_{wj}(C_{jb}\boldsymbol{\omega} + \boldsymbol{\Omega}_j) = \boldsymbol{T}_j + \boldsymbol{R}_j\end{aligned} \tag{5}$$

Along the 2_j axis on each wheel,

$$J_{rj}\left(c_{2j}^T\dot{\boldsymbol{\omega}} + \dot{\Omega}_j\right) = T_j \tag{6}$$

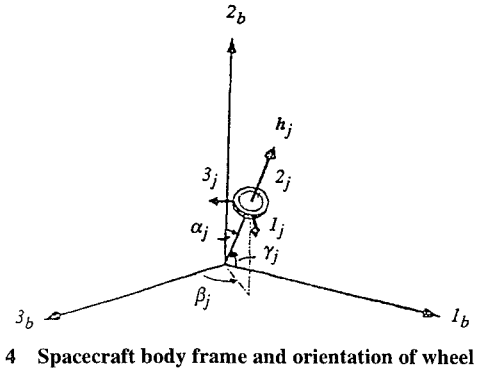

Fig. 4 Spacecraft body frame and orientation of wheel axis.

Finally, the following generalized equations of motion are derived:

$$\begin{aligned}\dot{\boldsymbol{\omega}} &= -J_s^{-1}[C\boldsymbol{T} + \boldsymbol{\omega}\times\boldsymbol{H}_T]\\ \dot{\boldsymbol{H}}_w &= C\boldsymbol{T}\end{aligned} \tag{7}$$

From now on, J_s is assumed to be diagonal and J_{rj} $(j = 1, \ldots, n)$ are all identical, with moment of inertia I_w. $\boldsymbol{H}_w$ is rewritten as follows:

$$\boldsymbol{H}_w = I_wC(C^T\boldsymbol{\omega} + \boldsymbol{\Omega}) \tag{8}$$

Closed Loop Control Law During Momentum Transfer Maneuver

A primary objective of an acquisition maneuver utilizing n wheels is not only transferring all of the angular momentum of the body to wheels but also establishing a desired state in which body rates are all attenuated and the spacecraft is motionless without any nutation. A closed-loop control strategy is inevitably introduced instead of an open-loop scheme. As already mentioned, an open-loop momentum transfer does not seem suitable for ASTRO-D, where minimum-to-maximum momentum transfer is requested, which may result in divergent and reversed motion or in falling into an equilibrium singular state.

Basically the idea adopted here is to generate torque commands for the wheels based on angular velocities around the body axes as well as differences between "prescribed" and current wheel spin rates. Prescribed wheel spin rates are the ultimate rates, determined by the final condition that all angular momentum be held only by wheels. When body angular rates are gradually attenuated, the resultant angular momentum held by wheels approaches the ultimate prescribed value. It is quite common that spacecraft are equipped with three axes gyros and that tachometers are available in wheel control circuits. Therefore, assumed control system here does not require any extra special device.

The authors have developed the following control law:

$$\boldsymbol{T} = -\{(K_b - K_a)\boldsymbol{\omega}_r + K_b(\boldsymbol{\Omega} - \boldsymbol{\Omega}_f)\}, \qquad \boldsymbol{\omega}_r = C^T\boldsymbol{\omega} \tag{9}$$

Both K_a and K_b here are positive scalar numbers and Eq. (9) still holds, remaining unchanged even when friction torque on the wheel driving mechanism is taken into account. Equation (9) is derived from feeding back the linear combination of both body and wheel error rates. Rewriting Eq. (9) in terms of K_a and K_b shows a straightforward interpretation of the idea. For the purpose of examining stability, a Lyapunov function is devised, as follows:

$$\begin{aligned}V &= K_a\tfrac{1}{2}\boldsymbol{\omega}^TJ_s\boldsymbol{\omega} + I_wK_b\tfrac{1}{2}\Delta\boldsymbol{\Omega}^T\Delta\boldsymbol{\Omega}\\ \Delta\boldsymbol{\Omega} &= \boldsymbol{\Omega} + \boldsymbol{\omega}_r - \boldsymbol{\Omega}_f\end{aligned} \tag{10}$$

It is shown that the Lyapunov function in Eq. (10) is positive definite and that its time derivative is easily reduced to the following form through the use of Eqs. (6), (7), and (9), yielding

$$\begin{aligned}\dot{V} &= -K_a\boldsymbol{\omega}^T(C\boldsymbol{T} + \boldsymbol{\omega}\times\boldsymbol{H}_T)\\ &\quad + I_wK_b(C^T\boldsymbol{\omega} + \boldsymbol{\Omega} - \boldsymbol{\Omega}_f)^T(C^T\dot{\boldsymbol{\omega}} + \dot{\boldsymbol{\Omega}})\\ &= -\boldsymbol{T}^2\end{aligned} \tag{11}$$

Equation (11) suggests that the time derivative of the Lyapunov function in Eq. (10) is negative semidefinite. Singular states annotated with an asterisk can be found to make Eq. (11), in other words Eq. (9), equal to zero.

Based on the equations of motion (6), the relation

$$\boldsymbol{\omega}^*\times\boldsymbol{H}_T^* = \mathbf{0} \tag{12}$$

holds and defines the general singular states solutions. Equating $\boldsymbol{\omega}^* = \xi\boldsymbol{H}_T^*$, in view of Eq. (4), first-type singular states are determined by solving the following equations, provided $P(\xi)$ exists:

$$\begin{aligned}&\boldsymbol{H}_T^* = P(\xi)\cdot\boldsymbol{H}_{wf}, \qquad \boldsymbol{H}_{wf} = CJ_r\boldsymbol{\Omega}_f\\ &P(\xi) = \left[\mathbf{1} - \xi\left(J_s - KCC^T\right)\right]^{-1}, \qquad K = -K_aI_w/K_b\end{aligned} \tag{13}$$

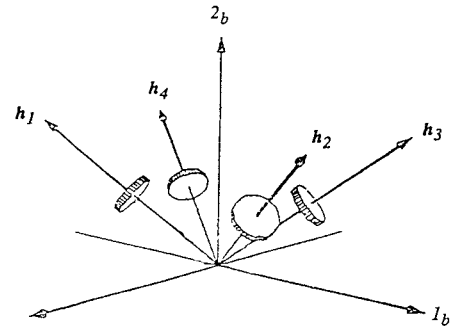

Fig. 5 Multiwheel configuration used for numerical demonstration.

The nominal target corresponds to the case of $\xi = 0$. Although this equation determines only the single nonzero real number ξ, corresponding to the steady state which is perfectly reverse to the nominal target, the other four (second and third types) solutions are found from both the equilibrium conditions shown next and Eq. (12). Note that $\boldsymbol{T}$ in Eq. (9) is constantly zero in steady state:

$$\omega^* = \left(J_s - KCC^T\right)^{-1}\left(\boldsymbol{H}_T^* - \boldsymbol{H}_{wf}\right) \tag{14}$$

The other four solutions correspond to ξ in which $P(\xi)$ does not exist and which denote the inversed eigenvalues of matrix $(J_s - KCC^T)$. As a result, there exist six equilibrium states, including the desired targeted one. $\boldsymbol{H}_T^*$ solutions are found as follows.

First type:

$$\boldsymbol{H}_{T1}^* = \{0, \pm H_T, 0\}^T \tag{15a}$$

Second type:

$$\boldsymbol{H}_{T2}^* = \{0, H_{T2y}, \pm H_{T2z}\}^T \tag{15b}$$

Third type:

$$\boldsymbol{H}_{T3}^* = \{\pm H_{T3x}, H_{T3y}, 0\}^T \tag{15c}$$

where

$$H_{T2y} = H_0\left(J_{33} - 2K\cos^2\gamma\right)\Big/\left[J_{33} - J_{22} - 2K(\cos^2\gamma - 2\sin^2\gamma)\right]$$

$$H_{T2z} = \left(H_0^2 - H_{T2y}^2\right)^{\frac{1}{2}}$$

$$H_{T3y} = H_0\left(J_{11} - 2K\cos^2\gamma\right)\Big/\left[J_{11} - J_{22} - 2K(\cos^2\gamma - 2\sin^2\gamma)\right]$$

$$H_{T3x} = \left(H_0^2 - H_{T3y}^2\right)^{\frac{1}{2}}$$

Here γ denotes the angle of the wheel rotor axis, which is the elevation angle from the 1_b–3_b plane as shown in Fig. 5. CC^T is assumed diagonal without loss of generality, which is the case when the wheel configuration in Fig. 5 is symmetric. It should be noted that all solutions to Eq. (12) subject to the law Eq. (9) will take the form of Eq. (15).

It should be stressed that these discussions are true of the single wheel case, taking γ as 90 deg. Six equilibrium states still exist even under such a configuration. Note also that $\boldsymbol{\Omega}_f$ here does not have to correspond to the ultimate wheel speed but can be an arbitrary targeted speed to aim for. The properties here remain unchanged, even though $\boldsymbol{\Omega}_f$ is an arbitrary speed. Even without any control, since the following relation similar to Eq. (14) holds, it is easily verified that generally six equilibrium states exist corresponding to the steady wheel spin rate $\boldsymbol{\Omega}^*$:

$$\omega^* = \left(J_s + I_w CC^T\right)^{-1}\left(\boldsymbol{H}_T^* - I_w C\boldsymbol{\Omega}^*\right) \tag{16}$$

Singular States Analyses

If $\boldsymbol{\Omega}_f$ is taken as an ultimate relative wheel speed with respect to the spacecraft body, virtual nutation angles θ_2 and θ_3 between steady-state total angular momentum vectors $\boldsymbol{H}_{T2y}(\boldsymbol{H}_{T3y})$ and the Y axis are expressed as

$$\cos\theta_2^* = \frac{J_{33} - 2K\cos^2\gamma}{J_{33} - J_{22} - 2K(\cos^2\gamma - 2\sin^2\gamma)}$$
$$\cos\theta_3^* = \frac{J_{11} - 2K\cos^2\gamma}{J_{11} - J_{22} - 2K(\cos^2\gamma - 2\sin^2\gamma)} \tag{17}$$

These solutions, which explicitly contain control parameter K, are first obtained and shown here. It is easily recognized that the necessary and sufficient conditions for equilibrium singular states to be avoided are

$$|\cos\theta_2^*| > 1, \qquad |\cos\theta_3^*| > 1 \tag{18}$$

Under the Eq. (18) conditions, the final destination is confined to type-1 equilibrium states. From a kinetic energy point of view, for two distinct equilibrium points belonging to type-1 states, the opposite solution corresponds to higher energy, therefore, the final destination must be the nominal trivial target. As far as the ultimate states are concerned, the conditions in Eq. (18) avoid an incomplete transfer. However, $\cos\theta_2$ and $\cos\theta_3$ should be greater than $+1.0$ and not lower than -1.0 in view of transient behavior.

In practical systems, since wheel driving torque is not infinite and $\boldsymbol{\Omega}_f$ in the control law (9) may be regarded to be raised gradually up to the ultimate state, the following equilibrium states may well be realized at every instance during the maneuver:

$$\frac{H_{T2y}(\Omega)}{H_0} = \cos\theta_2(\Omega) = \frac{J_{33} - 2K\cos^2\gamma}{J_{33} - J_{22} - 2K(\cos^2\gamma - 2\sin^2\gamma)} \cdot \frac{H_w(\Omega)}{H_0}$$
$$\frac{H_{T3y}(\Omega)}{H_0} = \cos\theta_3(\Omega) = \frac{J_{11} - 2K\cos^2\gamma}{J_{11} - J_{22} - 2K(\cos^2\gamma - 2\sin^2\gamma)} \cdot \frac{H_w(\Omega)}{H_0} \tag{19}$$

Provided that the singular points fade out in the 180-deg direction, as the wheel speed gets higher, virtual nutation angles θ_2 and θ_3 increase and show divergent behavior that sometimes seems a reversed reaction. This is the exact mechanism for how divergent motion takes place. In view of this, it is recognized that only Eq. (18) is not adequate for a successful transfer and that the equilibrium singularity should disappear toward the 0-deg direction. Therefore, more stringent conditions are derived as

$$\cos\theta_2^* > 1, \qquad \cos\theta_3^* > 1 \tag{20}$$

It is quite obvious that Eq. (20) is sufficient and more restrictive than Eq. (18).

As for the open-loop scheme, Eq. (17) may give another insight. A conventional open-loop transfer assumes constant torquing of a wheel, which can be expressed as a special case of Eq. (9). Suppose $K_a = 0$ and K_b stands for a saturator element, the control law (9) is degenerated to

$$\boldsymbol{T} = -K_b \cdot \left(C^T\omega + \boldsymbol{\Omega} - \boldsymbol{\Omega}_f\right) \cong -K_b \cdot (\boldsymbol{\Omega} - \boldsymbol{\Omega}_f) \tag{21}$$

This approximation holds while constant torque is applied to the rotor, during which torque command is not affected by body rate information. Discussions in regard to the Lyapunov function (10) still hold, and equilibrium states are simply defined as

$$\cos\theta_2^* = \frac{J_{33}}{J_{33} - J_{22}}, \qquad \cos\theta_3^* = \frac{J_{11}}{J_{11} - J_{22}} \tag{22}$$

here, θ_2 and θ_3 are completely dependent on the inertia properties and the following important characteristics are derived.

1) If $0.5 > (J_{33}/J_{22})$, then type-2 singularity exists.

2) If $1.0 > (J_{33}/J_{22}) > 0.5$, then type-2 singularity disappears in the 180-deg direction.

3) If $(J_{33}/J_{22}) > 1.0$, then type-2 singularity disappears in the 0-deg direction.

4) If $0.5 > (J_{11}/J_{22})$, then type-3 singularity exists.

5) If $1.0 > (J_{11}/J_{22}) > 0.5$, then type-3 singularity disappears in the 180-deg direction.

6) If $(J_{11}/J_{22}) > 1.0$, then type-3 singularity disappears in the 0-deg direction.

These six characteristics are compatible with previous results concerning open-loop transfer, which state that minor axis (2_b) shall be the destination. In the ASTRO-D spacecraft, $(J_{33}/J_{22}) = 0.34$ and $(J_{11}/J_{22}) = 0.98$. Since the type-2 singularity therefore exists, a closed control law is introduced. Only conditions 3 and 6 can circumvent divergent motion and shorten acquisition time in the open-loop schemes. The maneuver is governed only by inertia properties, and a major to minor transfer is preferable, as reported in Ref. 6.

On the other hand, in the closed control scheme, the situation is quite different. Since Eqs. (17) and (20) contain control parameter K, the inertia property can be improved virtually even when the case 2_b axis is that of maximum moment of inertia. As stressed in this paper, more stringent conditions to ensure that the singularity vanishes in the 0-deg direction are obtained through some manipulation,

$$-2K(\cos^2\gamma - 2\sin^2\gamma) > J_{22} - J_{33},\ J_{22} - J_{11} \tag{23}$$

To improve the "virtual" inertia property enough to exclude any divergent phenomenon, accepting that K must be negative for stability, γ shall be

$$\gamma < 35.26\,\text{deg} \tag{24}$$

Otherwise, even though intermediate equilibrium states may be avoided, divergence behavior is left unchanged. The single wheel configuration corresponds to the case of $\gamma = 90$ deg. The closed control method with single wheel system is not as effective as with a multiwheel system. Note that not all multiwheel configurations are effective in improving momentum transfer.

Obviously, when equilibrium points are excluded by choosing appropriate control parameters, the nominal target is the only destination, since the opposite attitude has higher kinetic energy. However, there is still a question of whether the intermediate equilibrium states are stable or not. Nothing has been noted so far in this paper about the stability around those equilibrium points. What follows will prove that all of the singular states are stable when K is taken as zero (in other words, in case only tachometer feedback is introduced). As for the cases in which K is not taken as zero, those are found to be saddle points qualitatively.

Temporarily assume an alternative Lyapunov function whose form is

$$V = \tfrac{1}{2}K_a\omega^T J_s\omega + (1/2I_w)K_b(\boldsymbol{H}_w - \boldsymbol{H}_{wf})^T(CC^T)^{-1}(\boldsymbol{H}_w - \boldsymbol{H}_{wf}) \tag{25}$$

Note that CC^T is nonsingular in the multiwheel configuration whose wheel assignment spans three-dimensional space. Although here it is implicitly assumed to be a multiwheel configuration, the same discussion is true of the single wheel system by appropriately altering the second term in Eq. (25). All of the properties concerning the Lyapunov function in Eq. (10) still hold even in this alternative form. Taking a small variation up to the second order of the Lyapunov function around singular states gives

$$\delta V = \left.\frac{\partial V}{\partial\omega}\right|_{\omega^*}\cdot\delta\omega + \left.\frac{\partial V}{\partial\boldsymbol{H}_w}\right|_{H_w^*}\cdot\delta\boldsymbol{H}_w + \frac{1}{2}\delta\omega^T\left(\frac{\partial^2 V}{\partial\omega^2}\right)_{\omega^*}\delta\omega + \frac{1}{2}\delta\boldsymbol{H}_w^T\left(\frac{\partial^2 V}{\partial\boldsymbol{H}_w^2}\right)_{H_w^*}\delta\boldsymbol{H}_w \tag{26}$$

Since the singularity condition satisfies the following relation according to Eqs. (9):

$$-K_a(CC^T)\omega^* + (K_b/I_w)(\boldsymbol{H}_w^* - \boldsymbol{H}_{wf}) = 0 \tag{27}$$

and according to Eq. (4) the second-order conservation of total angular momentum implies

$$\boldsymbol{H}_T^{*T}(J_s\delta\omega + \delta\boldsymbol{H}_w) + (J_s\delta\omega + \delta\boldsymbol{H}_w)^2 = \boldsymbol{0} \tag{28}$$

The variation of Lyapunov function is expressed as follows:

$$\begin{aligned}\delta V &= -\xi K_a(J_s\delta\omega + \delta\boldsymbol{H}_w)^T(J_s\delta\omega + \delta\boldsymbol{H}_w) \\ &\quad + (K_a/2)\delta\omega^T J_s\delta\omega + (K_b/2I_w)\delta\boldsymbol{H}_w^T(CC^T)^{-1}\delta\boldsymbol{H}_w \\ &= (J_s\delta\omega, \delta\boldsymbol{H}_w)^T \\ &\quad \cdot\begin{pmatrix} \frac{K_a}{2}(J_s^{-1} - 2\xi\mathbf{1}) & -\xi K_a\mathbf{1} \\ -\xi K_a\mathbf{1} & \frac{K_b}{2I_w}\{(CC^T)^{-1} + 2K\xi\mathbf{1}\}\end{pmatrix} \\ &\quad \cdot\begin{pmatrix} J_s\delta\omega \\ \delta\boldsymbol{H}_w\end{pmatrix}\end{aligned} \tag{29}$$

The ξ indicate the inverse of eigenvalues of $(J_s - KCC^T)$ matrix as discussed earlier. It should be noted that this manipulation does not assume linearization but is made rigorously in second order.

The most straightforward result is obtained by taking K_a as zero, which corresponds to $K = 0$. In this case, the local Lyapunov surface is convex in three-dimensional subspace but flat in other three-dimensional subspace. As a result, it is concluded here that all of the equilibrium states are stable in the case where K is taken as zero. When the same discussion is applied to a single wheel system, the same conclusion is obtained, which states that only a tachometer feedback control can not enable escape from intermediate equilibrium states. In general, the local properties of the Lyapunov function are governed by the eigenvalues of the matrix in Eq. (29) which constitute a quadratic form. The details are omitted here, but, qualitatively, the discussion here concludes that this matrix contains both negative and positive eigenvalues in the case when K is not zero, which indicates that the singular points are saddle points.

Numerical Demonstrations

A numerical demonstration is given here for the ASTRO-D spacecraft, whose preflight configuration parameters are listed in Table 1. Wheel orientation is the same as in Fig. 5.

As is easily verified, $(J_{33}/J_{22}) = 0.34$, $(J_{11}/J_{22}) = 0.98$. Obviously, under either the open-loop scheme or the insufficient closed-loop control type-2 ultimate equilibrium states exist, whereas the third type disappears in the 180-deg direction. As a first illustration, assume the control parameters to be $K_a = 0.059$ Nms/rad and $K_b = 0.00064$ Nms/rad, which is converted to $K = -1.51$ kgm^2. Figure 6 shows the typical results, assuming a torque limit up to 0.002 Nm. Transfer angle here denotes the virtual nutation angle between the Y axis and the total angular momentum vector $\boldsymbol{H}_T$, in body-fixed coordinates. As anticipated from Eq. (22) in the preceding section, the transfer falls into an equilibrium state whose nutation angle is 122.1 deg, which is exactly compatible with the analyses given earlier. Slight instability around this equilibrium point should be noted here. In an extraordinary period, angular momentum vector $\boldsymbol{H}_T$ escapes from this singularity and is aligned to the nominal target. Since this singular point has higher kinetic energy than that of the nominal

Table 1 Attitude control parameters in ASTRO-D

$J_{11} = 294$ kgm^2, $J_{22} = 299$ kgm^2, $J_{33} = 102$ kgm^2
$J_{rj} = 0.0164$ kgm^2, $(j = 1, 2, 3, 4) = I_w$
$\gamma = 30$ deg, $\alpha_j = 60$ deg, $\beta_j = \pi/4 + \pi/2(j-1)$
$K_a = 0.059135$ Nms/rad, $K_b = 0.00064$ Nms/rad
$\Omega_{fj} = 2000$ rpm $(j = 1, 2, 3, 4)$

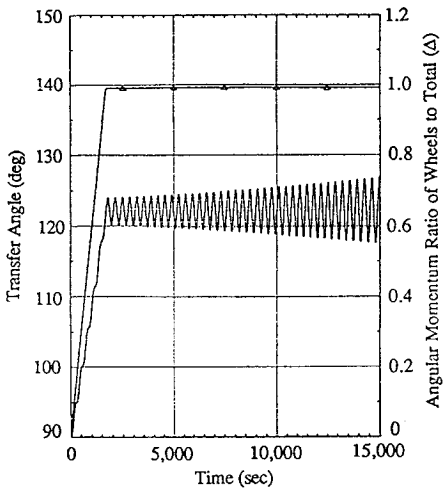

Fig. 6 Insufficient closed-loop control falling into equilibrium state.

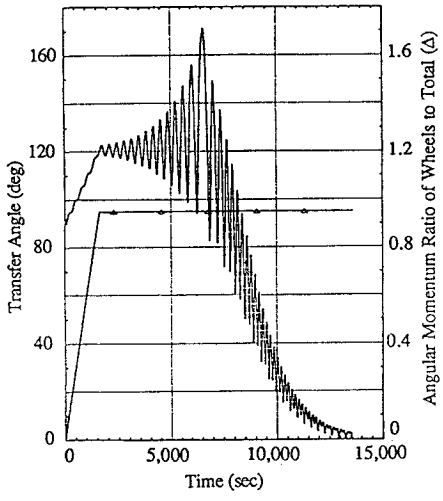

Fig. 7 Escape from equilibrium with damper.

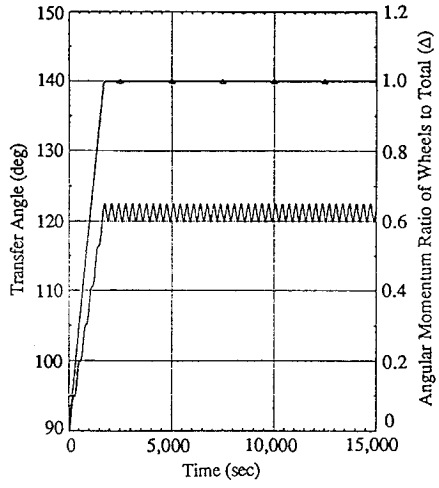

Fig. 8 Equilibrium states, $K = 0$.

target, with some active dissipation mechanism $\boldsymbol{H}_T$ easily departs from this trap, which is depicted in Fig. 7 where the wheels are spun up to the 95% level of the entire angular momentum. As an illustration of the analyses made in the previous section concerning stability around equilibrium states, simulation results in which $K_a = 0$ Nms/rad and $K_b = 0.00064$ Nms/rad are shown in Fig. 8. As proved before, once the path falls into an equilibrium state whose nutation angle is 121.2 deg, it never seems to get rid of it, keeping oscillation with constant amplitude without a damper. In addition, direct numerical simulations which depart from the vicinity of first and second type singular points are carried out, and their results are summarized

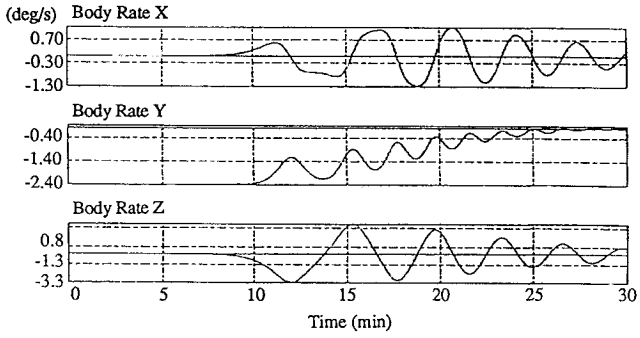

Fig. 9 Simulation with the initial condition close to first type singular state.

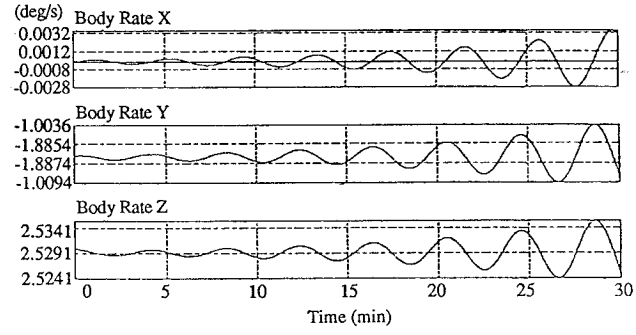

Fig. 10 Simulation with the initial condition close to second type singular state.

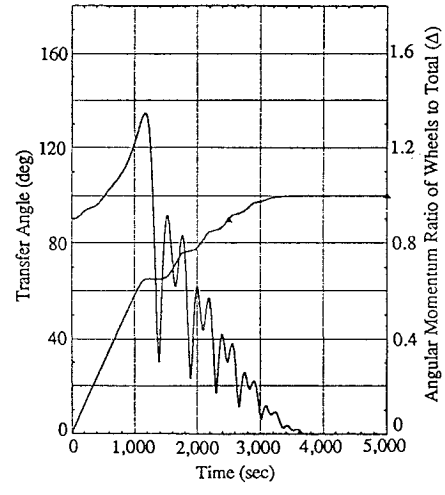

Fig. 11 Elimination of singular state, $K = -65.6$ kgm^2.

in Figs. 9 and 10. When started from the attitude opposite to the nominal target, the path immediately diverges to the nominal destination. However, when started from the second type of equilibrium state, a slight instability is observed, which corresponds to Fig. 6. All of these numerical examples support the discussion made here.

According to Eq. (17), the virtual moment of inertia over 47.5 kgm^2 is found to exclude a type-2 singularity. Figure 11 shows the simulation results taking $K_a = 0.4$ Nms/rad and $K_b = 0.0001$ Nms/rad, which are converted to -65.6 kgm^2 in K. As expected, at the beginning phase of the transfer, the virtual nutation angle diverges to the opposite direction, however, $\boldsymbol{H}_T$ converges to the nominal target in a relatively shorter period. As Eq. (23) indicates, a virtual moment of inertia over 394 kgm^2 avoids not only intermediate equilibrium states but divergent motion as well. Figures 12 and 13 show the angular momentum vector history with control parameters $K_a = 1.0$ Nms/rad and $K_b = 0.00004$ Nms/rad ($K = -410$ kgm^2). In Fig. 12, a torque limiter of 0.002 Nm is turned on, whereas no saturation mechanism is included in the case in Fig. 13. When a torque saturator is introduced, no distinction occurs during the initial spinup phase from a controller with smaller

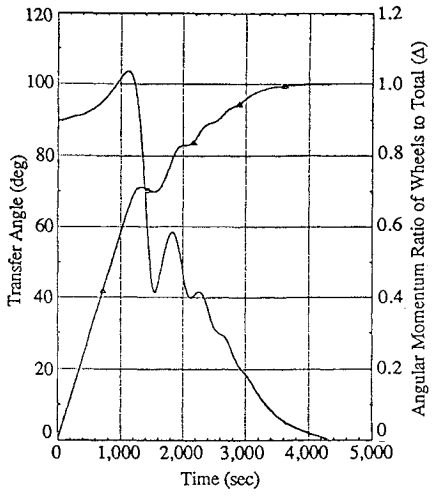

Fig. 12 Full compensation with torque limiter, $K = -410$ kgm^2.

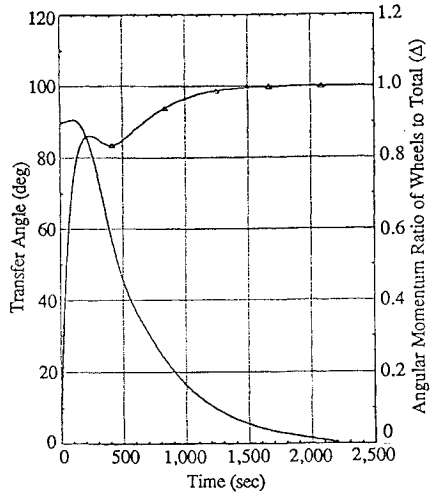

Fig. 13 Full compensation without torque limiter, $K = -410$ kgm^2.

virtual moment of inertia, yet the divergent feature is still observed even under the controller with extraordinary high virtual moment of inertia. Figure 13 numerically confirms the theoretical discussion showing no divergent path even at the beginning phase. However, the peak torque in Fig. 13 is up to 0.02 Nm, which is 10 times as high as the torque in Fig. 12.

Comparison between Figs. 11 and 12 suggests interesting characteristics that are important in a practical manner. Whereas a reversed overshoot is greater in Fig. 11 than in Fig. 12, acquisition time in Fig. 11 is shorter than in Fig. 12. This is mainly caused by higher feedback gain K_a against body motion in the case in Fig. 12. From a practical point of view, since torque saturation is inevitably included more or less in the feedback loop and some noise in gyros might effect control performance, a compromised design should be considered.

In the actual flight, control parameters K_a and K_b were determined in view of practical aspects such as gyro noise, which never assure the elimination of singular states. Figure 14 shows the flight results, in which nutation angle history is plotted. Inertia properties of the flight model were varied: $J_{11} = 332$ kgm^2, $J_{22} = 328$ kgm^2, $J_{33} = 102$ kgm^2 and a minimum to intermediate transfer was carried out. Control parameters K_a and K_b were set as 0.59087 Nms/rad and 0.000605 Nms/rad, respectively. Resultant K is -16.017 kgm^2, which never excludes the second type singular states, and the anticipated equilibrium nutation angle was 125.2 deg. The decision was made to circumvent too high feedback gain for body rates, so that noise cannot degrade the control performance. The nutation frequency observed is different from that simulated in Fig. 7, since Fig. 14 gives nutation motion viewed in body-fixed coordinates, whereas Fig. 7 shows it in the inertial frame. Frequency observed is 2.2 times faster than that in Fig. 7. Torque limiter in the actual

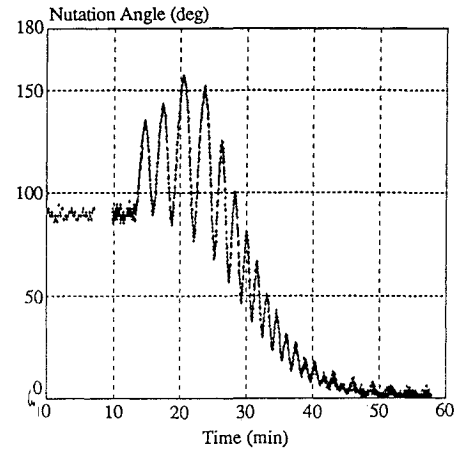

Fig. 14 Flight results, nutation angle.

hardware was 0.066 Nm and the wheels were spun up much faster than those in the numerical simulations shown so far. It should be noted that similar to Fig. 7 nutation diverges first to the equilibrium state of 125.2 deg, which is damped by passive energy dissipation, whose time constant is close to what was demonstrated in Fig. 7. Unfortunately, ideal parameters for full compensation were not actually taken, however, the results here strongly support the effectiveness of the proposed control scheme and prove the practical feasibility.

Conclusion

Automatic control laws for momentum transfer maneuver were discussed and applied to the ASTRO-D X-ray telescope spacecraft. Since solar cell panels are attached to ASTRO-D's Y axis, the angular momentum vector is required to lie toward the Y axis. Launch configuration restricts the spin axis to be the Z axis with minimum moment of inertia and a momentum transfer maneuver to shift the angular momentum vector from the Z to Y axis is planned. An open-loop momentum transfer does not seem appropriate in the ASTRO-D case, since a rapid transfer is required.

Intensive attention has been focused on stability analysis of this automatic maneuver based on the Lyapunov theorem. Universal asymptotic stability has been proved except at special points. Discussions have been concentrated on singular states, where any decrease in the Lyapunov function does not occur and the controller does not work. It has been revealed that, in general, six equilibrium states that are singular states exist if a closed-loop momentum transfer is attempted, including the nominal desired target. They are classified in three types, each of which consists of two equilibrium states. The first type singularity always appears, whereas the second and third singularities sometimes disappear. One of the first type singular states is almost meaningless from a practical point of view, since it corresponds to the point opposite the nominal target. Most crucial are the second singularities, which lie in the domain of practical use.

Here is proposed a new closed-loop control law that stabilizes this maneuver using four wheels. Equilibrium states are derived explicitly in terms of control parameters, and sufficient conditions are provided, which circumvent such singular states as well as divergent motion by an appropriate choice of control parameters. It is also noted here that closed control in a single wheel system is not of much practical use, since it does not improve the virtual inertia property. As to wheel configuration, it is found that not all multiwheel configurations are effective to this end.

Numerical examples are shown for ASTRO-D spacecraft. Simulations show that the closed-loop control law proposed here avoids singular states and divergent motion, through which the tuning rule of control parameters is perfectly proved.

References

[1]Cochran, J. E., "Nonlinear Resonances in the Attitude Motion of Dual-Spin Spacecraft," *Journal of Spacecraft and Rockets*, Vol. 14, No. 9, 1977, pp. 562–572.

[2]Cochran, J. E., and Beaty, J. R., "Near-Resonant and Transition Attitude Motion of a Class of Dual-Spin Spacecraft," *Journal of the Astronautical Sciences*, Vol. 26, No. 1, 1978, pp. 19–45.

[3]Cochran, J. E., Shu, P. H., and Rew, S. D., "Attitude Motion of Asymmetric Dual-Spin Spacecraft," *Journal of Guidance, Control, and Dynamics*, Vol. 5, No. 1, 1982, pp. 37–42.

[4]Scher, M. P., and Farrenkopf, R. L., "Dynamic Trap States of Dual-Spin Spacecraft," *AIAA Journal*, Vol. 12, No. 12, 1974, pp. 1721–1725.

[5]Gebman, J. R., and Mingori, D. L., "Perturbation Solution for the Flat Spin Recovery of a Dual-Spin Spacecraft," *AIAA Journal*, Vol. 14, No. 7, 1976, pp. 859–867.

[6]Hubert, C., "Spacecraft Attitude Acquisition from an Arbitrary Spinning or Tumbling State," *Journal of Guidance and Control*, Vol. 4, No. 2, 1981, pp. 164–170.

[7]Li, T., and Longman, W., "Stability Relationships Between Gyrostats with Free, Constant-Speed, and Speed-Controlled Rotors," *Journal of Guidance, Control, and Dynamics*, Vol. 5, No. 6, 1982, pp. 545–552.

[8]Guelman, M., "On Gyrostat Dynamics and Recovery," *Journal of the Astronautical Sciences*, Vol. 37, No. 2, 1989, pp. 109–119.

[9]Ninomiya, K., Uo, M., Maeda, K., and Saitoh, T., "Attitude Control System of the X-ray Observatory ASTRO-D," *Proceedings of 11th International Federation of Automatic Control World Congress*, Vol. 1, 1990, pp. 101–106.

[10]Weisberg, J., and Ninomiya, K., "Improved Method for Initial Attitude Acquisition Maneuver," *Journal of Guidance, Control, and Dynamics*, Vol. 10, No. 3, 1987, pp. 316–319.

[11]Song, J. D., "Attitude Acquisition Maneuver for Bias Momentum Spacecraft with Multi-Wheels," Ph.D. Thesis, Dept. of Engineering, Univ. of Tokyo, Japan, March 1990.

[12]Maeda, K., Ninomiya, K., and Kawaguchi, J., "A New Control Law for Satellite Momentum Transfer in its Attitude Acquisition," *Proceedings of 12th International Federation of Automatic Control Symposium on Automatic Control in Aerospace Control '92* (Ottobrunn, Germany), 1992, pp. 183–188.

[13]Song, J. D., et al., "On the Momentum Transfer Maneuver for Initial Acquisition Using Multi-Wheels—Its Analysis and Application," *Proceedings of AIAA Guidance, Navigation, and Control Conference*, AIAA, Washington, DC, 1992, pp. 1583–1589 (AIAA Paper 92-4332).